Definitely not a circle: on the variability of the zone of influence in porous media flows

Michelle Boham[†] and Yana Nec[†]

[†] Department of Mathematics and Statistics, Thompson Rivers University, British Columbia, Canada.

Abstract

When fluid motion is induced through a porous medium, the distance travelled depends on the energy exerted and overall resistance to flow. Ostensibly intuitive, this concept of reach has proven elusive not only in delineation, but even mathematical definition. In wells surrounded by a homogeneous medium it is a circle and thus characterised by a single number referred to as the radius of influence. The simple definition thereof as the locus of zero radial velocity yields an infinite or severely overestimated result, and tempts custom modifications to reconcile the estimates with reality. In environmental applications such as aquifer sparging wells, hydraulic and petroleum wells, natural gas and landfill gas wells, the medium is often highly heterogeneous. The analysis presented herein shows that the zone of collection or dispersal changes shape dramatically based on the interrelation of resistance to flow posed by subdomains of distinct permeabilities. In contrast to the isotropic case, the mere presence of heterogeneity suggests a natural and unambiguous definition of this zone of interest as a set of separatrices connecting stagnation points in the flow field, and results in realistic estimates. The variability of its shape is remarkable and relates to the structural diversity of the parameter space underpinning the flow field. The findings help explain the longstanding problem of a reliable delimitation of these wells' reach in practice.

1 Background

When fluid flow is induced within a porous medium via injection or suction, the well's reach might be loosely defined as the region of motion in the desired direction – outwards in contaminated aquifer sparging wells and inwards in extraction wells. To this day fundamental aspects of the wells' operating principles remain equivocal: theoretical models match laboratory experiments on small scale substrates of idealised particles (McCray and Falta, 2005), but perform inadequately when applied to large environmental systems, and wells continue to be designed based on experience rather than accurate modelling (Houben, 2015). The classical fluid flow visualisation is via velocity or pressure profiles or contours in either longitudinal or cross-sectional view. Depending on the cut plane and the industrial application, a concept of the well's reach might be defined in a variety of ways. Figure 1 depicts typical examples. The profile in the longitudinal view (left panel) might represent the surface formed by the body of fluid in response to pumping or a profile of pressure or velocity when moving radially outwards from the well. The contour in the transversal projection (right panel) might demarcate the area wherefrom fluid is collected, or be an isocontour of pressure or velocity. In sparging wells it would correspond to area of dispersal or isocontour of detected concentration of the injected compounds. In practice the decision on the adequate cut-off for a residual pressure gradient, velocity or concentration depends on the application and experience with the site.

The desire to create easily tractable mathematical models in the case of environmental porous media flows has historically resulted in oversimplified and thus impractical descriptions. In hydraulic wells the planar zone of capture is defined as the transversal cross-section area, where all particle pathlines eventuate in the well. A group of analytical models uses complex potential to obtain streamlines, avoiding medium properties altogether and predicting an open-ended zone, i.e. the pathlines originate infinitely far away (Javandel and Tsang, 1986; Kompani-Zare et al., 2005; Asadi-Aghbolaghi et al., 2011). The concept of

drawdown complements the zone of capture by looking at the vertical profile of the water surface, but the exact definition thereof is not straightforward (Pechstein et al., 2016). In petroleum wells the more common term used is the radius of investigation or radius of disturbance, defined as the area where the head induced at the well is traceable. Unfortunately, the simplest steady state Darcy flow gives a monotonic pressure profile, rendering the threshold of traceability subjective. In the field different empirical formulae are used, including ones that specify when to transition from the flow field predicting an infinite reach to a more sophisticated description resulting in a finite radius (Kuchuk, 2009; Sobbi and Badakhshan, 1996). A similar concept exists in gas wells, but with possible distinction between the radius of influence and radius of investigation (Bresciani et al., 2020). The interest in suitable modifications of these tractable, but unrealistic flow models has not abated in decades (Podgorney, Jr. and Ritzi, 1997; Xu and van Tonder, 2002; Bakr and Butler, 2004; Ataie-Ashtiani et al., 2012; Frind and Molson, 2018). This is particularly true in applications with compressible fluids (Al-Hussainy et al., 1966; Nec and Huculak, 2019; Halvorsen et al., 2019), as low Reynolds numbers render non-linear momentum transfer models, such as Forchheimer (Whitaker, 1996) or Brinkman (Brinkman, 1947; Durlofsky and Brady, 1987) equations, unavailing. Varying permeability as a way to alter transport efficiency has only recently come into focus (Awasthi et al., 2023; Benner et al., 2002; Hyman et al., 2015; Zhang et al., 2022). In unsteady flow the definition and estimation of the zone of influence are somewhat easier, albeit still far from trivial (Benner et al., 2002; McCray and Falta, 1996).

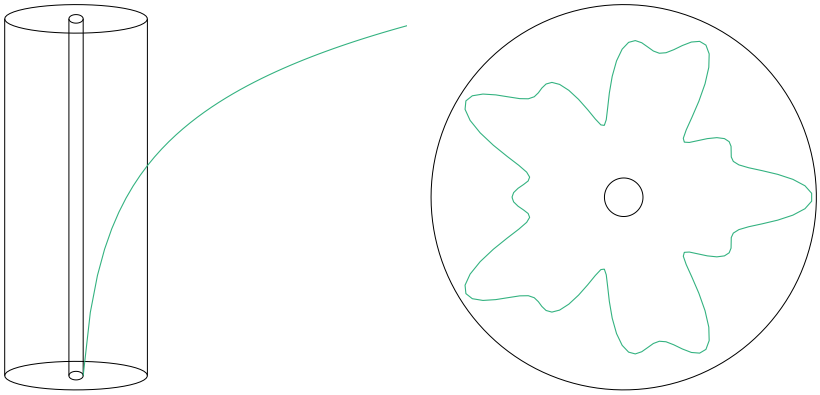

Figure 1: Schematic of longitudinal (left) and transversal (right) types of well reach definitions: well and surrounding substrate bounds (inner and outer cylinder / circle, black); profile or contour (green / grey).

Under steady conditions no unambiguous universal framework exists, although it is indisputable that finite energy input at the well must result in a finite reach. All aforesaid types of zones of interest are interrelated, since induced pressure gradient must result in fluid flow. The terms *zone of capture* and *zone of influence* are conventionally applied to visualisation via pathlines and pressure profiles respectively. This study revisits the concept of the well's reach and proposes a medium heterogeneity based method applicable to most types of wells with the aim to establish a theoretical framework that is simple to use, provides realistic estimates and circumvents the ambiguities entailed by empirical approaches. The methodology commingles the use of an analytically obtained pressure field and numerically integrated pathlines. The initial concept was motivated by the problem of landfill gas collection, where the well's reach is referred to as the zone of influence, and this terminology is adopted throughout. Nevertheless, the model is generic and applicable to any flow induced within an unidealised porous medium, and the reader should interpret the results regarding the zone of interest accordingly.

2 Flow field

A steady mass conservation equation in a porous medium is identical to that of a continuum flow of fluid of density ρ and velocity $\mathbf{u}$ subject to bulk generation rate C (Fulks et al., 1971):

$$\nabla \cdot (\rho \mathbf{u}) = C. \tag{1a}$$

The momentum transfer is governed by Darcy's law (Whitaker, 1986):

$$\mathbf{u} = -\frac{1}{\mu}\,\bar{\bar{K}}\nabla p, \tag{1b}$$

where μ and p denote fluid viscosity and pressure respectively, and $\bar{\bar{K}}$ is the permeability tensor. Measurements in vertical wells indicate the zone of influence is depth dependent (Agarwal et al., 2005; Lundegard and LaBrecque, 1995). In horizontal wells it similarly varies longitudinally due to head loss upstream from the outlet (Nec and Huculak, 2019). The mainstay concept of the solution construction to be demonstrated is reliant on an azimuthal variability of the medium properties. Therefore the analysis focusses on a planar transversal cross-section, be the well horizontal or vertical, and the gravity potential was not included in (1b). Since any well's primary purpose is to induce radial transport, it is convenient to use the polar coordinates (r, θ). This choice does not imply the domain must be circular, and the solutions constructed below might be extended to a domain of an arbitrary shape. Then $\mathbf{u} = (u, v)^{\mathrm{T}}$ with u and v denoting the radial and azimuthal velocity components, and the permeability tensor is given by

$$\bar{\bar{K}} = \begin{pmatrix} k_r & 0 \\ 0 & k_\theta \end{pmatrix} \tag{1c}$$

with k_r and k_θ standing for effective values in the respective directions. The theory introduced infra is easily generalised to a tridimensional space, but would require setting boundary conditions in the longitudinal direction z, which differ between applications. The associated numerical implementation and flow visualisation, however, are beyond the ambit of this study.

If the fluid is incompressible, the density ρ is constant. In the case of gas flow an equation of state relates p and ρ. In most large scale geophysical and environmental systems the thermodynamic conditions allow for the use of the ideal gas equation of state

$$p = \rho R T, \tag{1d}$$

where R is the specific gas constant and T – temperature. Combine (1) into a single equation in the fluid pressure p:

$$\frac{\partial}{\partial r}\left(k_r r \frac{\partial p^\gamma}{\partial r}\right) + \frac{1}{r}\frac{\partial}{\partial \theta}\left(k_\theta \frac{\partial p^\gamma}{\partial \theta}\right) = -\tilde{C} r, \tag{2a}$$

$$\tilde{C} = \tilde{\gamma} C, \qquad \tilde{\gamma} = \begin{cases} \gamma\mu/\rho & \gamma = 1 \\ \gamma\mu R T & \gamma = 2, \end{cases} \tag{2b}$$

where $\gamma = 1$ and $\gamma = 2$ correspond to the incompressible and compressible cases respectively. Introduce dimensionless quantities by mapping $\bar{\bar{K}} \longmapsto r_x^2 \bar{\bar{K}}$, $p \longmapsto p_s p$ and $\tilde{C} \longmapsto p_s^\gamma \tilde{C}$ with r_x and p_s standing for characteristic length and pressure scales. Herein r_x was taken to be the computational domain radius and p_s – standard atmospheric pressure. Equation (2a) arises in numerous problems in physics and engineering outside of the field of porous media flows with the non-linearity parameter γ attaining a range of values, including negative and fractional. For a recent comprehensive review the reader is referred to (Awasthi et al., 2023). Hereunder the tilde in $\tilde{C}$ is omitted for simplicity.

An axially symmetric solution of (2a) is given by

$$p^\gamma = -\frac{C}{4k_r}\, r^2 + a \ln r + b \tag{3}$$

with a and b integration constants. Note that the assumption of axial symmetry automatically implies a medium that is both homogeneous and isotropic. Solution (3) was derived for $\gamma = 2$ in (Wise and Townsend, 2011), but the generalisation to an arbitrary γ is immediate. The point of velocity reversal is the root of $\partial_r p = 0$ and yields the radius of influence as

$$r_{\circledcirc} = \sqrt{2k_r a/C}\,. \tag{4}$$

In landfill gas wells $a > 0$ and $C > 0$ with the pressure increasing monotonically whilst $r < r_{\circledcirc}$, and thenceforth the fluid flows outwards and pressure diminishes. In sparging wells $a < 0$ and $C < 0$ since the remediating reaction removes the injected compounds, and flow trends are reversed. In both cases $|C| \ll 1$, implying that $r_{\circledcirc} \gg 1$ and entailing a gross overestimation that renders this simple model unusable in practice (Lundegard and LaBrecque, 1995; Vigneault et al., 2004). In natural gas wells if the fluid is generated within the medium it flows through, the situation is identical to that of landfill gas flow. If the fluid traverses a non-generating substrate on its way to the well, $C = 0$, the pressure profile is monotonic throughout and $r_{\circledcirc} = \infty$. This also applies to incompressible fluids such as water and petroleum. The technical question is how a varies as $C \longrightarrow 0$. It will be shown hereinafter that the ratio a/C grows infinitely at this limit. The inadequacy of this description was recognised many decades ago. Attempts to improve the estimates, from early works targeting a better compressibility description (Al-Hussainy et al., 1966) to amendments to the definition of the radius of influence itself (Bresciani et al., 2020) are collectively unconvincing in the sense that no overarching approach was found to be sufficiently robust to encompass all applications governed by (2a). A common practical method is to define a cut-off threshold of small $\partial_r p$ (zone of influence), or one of $|u|$, $\|\mathbf{u}\|$ or $|u|/\|\mathbf{u}\|$ (zone of capture). Not only is the threshold magnitude a site specific and often subjective choice, even more telling is the fact that the residual physical quantity itself is not unequivocal.

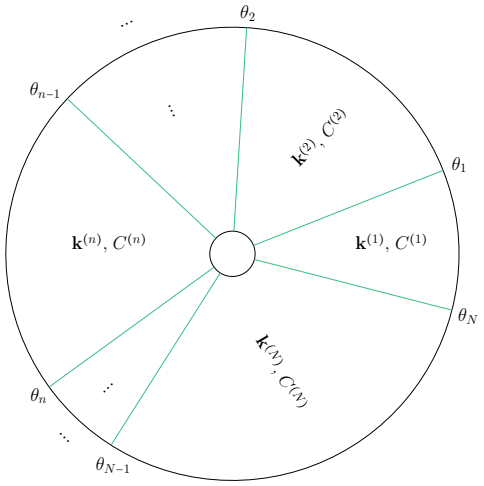

Figure 2: Flow domain schematic: indexing of contiguity rays θ_n and intrinsic porous matrix properties $\mathbf{k}^{(n)} = \left(k_r^{(n)}, k_\theta^{(n)}\right)$, $C^{(n)}$, $1 \leqslant n \leqslant N$.

Herein an alternative approach is set forth based on the premise of medium heterogeneity and/or anisotropy. Measurements performed in aquifers and landfills are plagued with inconsistent recorded results, whose interpretation is further undermined by the ingrained assumption the zone of influence must be circular (Agarwal et al., 2005; Lee et al., 2016; Lundegard and LaBrecque, 1995; McCray and Falta, 2005;

Vigneault et al., 2004). A recent analysis shows that the mathematical system governing the flow through a heterogeneous porous medium is subject to certain structural singularities that in practice translate to inconsistent behaviour (Nec, 2021). When the medium contains small subdomains of disparate permeability, the likelihood of stumbling close to such a singularity is tangible, especially when changes in water table level and ambient conditions occur where the substrate is prone to saturation, or when fissures open preferential directions of flow, be it natural (Gingras et al., 2022; Hyman et al., 2015) or introduced artificially by methods such as hydraulic fracturing. The current study proposes an unambiguous definition of the zone of influence that takes into account the spatial variability of the medium properties and provides robust realistic estimates. The findings comprehensively explain the difficulties encountered in practice to delineate the zone of influence reliably. With the relaxation of the constraint of axial symmetry its shape ceases being circular and instead depends on the mosaic of subdomains of distinct permeabilities. The diversity of the zone's shape and orientation underscores the crippling limitation harboured by axially symmetric modelling in the presence of even mild heterogeneity.

In a planar cross-section of the substrate near the well it is possible to designate azimuthally oriented subdomains with distinct effective permeabilities $\mathbf{k}^{(n)} = \left(k_r^{(n)}, k_\theta^{(n)}\right)$ and/or generation rates $C^{(n)}$, $1 \leqslant n \leqslant N$. For instance, a preferential direction of flow might be represented by a narrow sector of a higher permeability (Bradbury and Muldoon, 1994). Figure 2 depicts such a partition. The number of sectors N and their angles θ_n are arbitrary, but no attempt should be made to create a continuous variation via either an infinite N or infinitesimally close θ_n. The first step is to solve (2a) within each sector via the standard separation of variables technique:

$$p^\gamma = A(r)B(\theta) - \frac{C}{4k_r}\, r^2, \tag{5a}$$

resulting in

$$r^2 A'' + rA' - \frac{k_r}{k_\theta}\alpha^2 A = 0, \qquad B'' + \alpha^2 B = 0, \tag{5b}$$

where $\alpha^2 \geqslant 0$ is a separation constant. The function $B(\theta)$ must be 2π-periodic, yielding $\alpha = m$, $m \in \mathbb{N}$, and $B \in \operatorname{span}\left\{\sin(m\theta), \cos(m\theta)\right\}$, $A \in \operatorname{span}\left\{r^{\tilde{m}}, r^{-\tilde{m}}\right\}$ with $\tilde{m} = m\sqrt{k_r/k_\theta}$. The case $\alpha = 0$ completes the eigenbasis with $B \equiv 1$ and $A \in \operatorname{span}\left\{1, \ln r\right\}$. Then the most general solution within a single sector is given by

$$p_n^\gamma = \frac{C^{(n)}}{4k_r^{(n)}}\Bigg\{ - r^2 + b_{1_0}^{(n)} + b_{2_0}^{(n)} \ln r + \sum_{m=1}^{\infty}\left(r^{\tilde{m}}\left(a_{1_m}^{(n)}\sin(m\theta) + b_{1_m}^{(n)}\cos(m\theta)\right) + r^{-\tilde{m}}\left(a_{2_m}^{(n)}\sin(m\theta) + b_{2_m}^{(n)}\cos(m\theta)\right)\right)\Bigg\} \tag{6}$$

with $a_{i_m}^{(n)}$ and $b_{i_m}^{(n)}$, $i = \{1, 2\}$, integration constants. The case $k_r/k_\theta = 1$ was studied in (Nec, 2021). Writing the factor $C^{(n)}\big/\left(4k_r^{(n)}\right)$ outside of the curly braces is convenient when $C^{(n)} \neq 0$. When $C^{(n)} = 0$, the generation term vanishes and it is more expedient to drop this factor. Since only the ratio $C^{(n)}\big/k_r^{(n)}$ appears in (6), define a uniform generation rate C_* and map $k_r^{(n)} \longmapsto k_r^{(n)} C_*\big/C^{(n)}$. Henceforth $C^{(n)} = C_*$ and the asterisk is omitted for simplicity. For p to be a continuous function the equality

$$p_n\big|_{\theta_n} = p_{n+1}\big|_{\theta_n}, \quad 1 \leqslant n \leqslant N, \tag{7a}$$

must hold on all contiguity rays θ_n, where $N+1$ maps to 1 due to periodicity. Conservation of mass across a ray demands that

$$k_\theta^{(n)}\partial_\theta p_n\Big|_{\theta_n} = k_\theta^{(n+1)}\partial_\theta p_{n+1}\Big|_{\theta_n}, \quad 1 \leqslant n \leqslant N, \tag{7b}$$

with a similar periodic closure. Equation (7b) is obtained by integrating (2a) in the θ direction along an infinitesimal arc $(\theta_n - \varepsilon, \theta_n + \varepsilon)$ straddling a ray θ_n, taking the limit $\varepsilon \longrightarrow 0$ and using (7a). For $m \geqslant 1$ arrange the constants $a_{im}^{(n)}$ and $b_{im}^{(n)}$ (separately for each i) as

$$\mathbf{c} = \begin{pmatrix} a_{im}^{(1)} & b_{im}^{(1)} & \cdots & \cdots & a_{m}^{(N)} & b_{im}^{(N)} \end{pmatrix}^{\mathrm{T}}. \tag{8a}$$

Then equations (7) comprise a linear system

$$\mathfrak{C}\mathbf{c} = \mathbf{r}, \tag{8b}$$

wherein the matrix $\mathfrak{C}$ is almost block-bidiagonal

$$\mathfrak{C} = \begin{pmatrix} \mathfrak{A}_1 & \mathfrak{B}_1 & & & \\ & \mathfrak{A}_2 & \mathfrak{B}_2 & & \\ & & \ddots & \ddots & \\ & & & \mathfrak{A}_{N-1} & \mathfrak{B}_{N-1} \\ \mathfrak{B}_N & & & & \mathfrak{A}_N \end{pmatrix} \tag{8c}$$

with the block matrices defined by

$$\mathfrak{A}_n = \begin{pmatrix} \sin(m\theta_n) & \cos(m\theta_n) \\ \cos(m\theta_n) & -\sin(m\theta_n) \end{pmatrix}, \tag{8d}$$

$$\mathfrak{B}_n = \frac{\tilde{k}_r^{(n)}}{\tilde{k}_\theta^{(n)}} \begin{pmatrix} -\tilde{k}_\theta^{(n)} \sin(m\theta_n) & -\tilde{k}_\theta^{(n)} \cos(m\theta_n) \\ -\cos(m\theta_n) & \sin(m\theta_n) \end{pmatrix} \tag{8e}$$

and $\tilde{k}_r^{(n)} = k_r^{(n)} \big/ k_r^{(n+1)}$, $\tilde{k}_\theta^{(n)} = k_\theta^{(n)} \big/ k_\theta^{(n+1)}$.

The right-hand side vector $\mathbf{r}$ in (8b) depends on the anisotropy ratio k_r/k_θ that determines the powers $\tilde{m}$ in (6). First suppose that $k_r/k_\theta = 1$. Then for $m = 2$ the eigenfunction $r^{\tilde{m}}$ matches the generation term r^2, yielding

$$\mathbf{r} = \begin{pmatrix} 1 - \tilde{k}_r^{(1)} & 0 & \cdots & \cdots & 1 - \tilde{k}_r^{(N)} & 0 \end{pmatrix}^{\mathrm{T}}, \tag{9}$$

but $\mathbf{r} = \mathbf{0}$ for all other $m \geqslant 1$. The harmonic $m = 2$ is essential, because if equation (8b) possesses no solution, the construction of the heterogeneous flow field fails. A necessary and sufficient condition of the solvability of (8b) is $\det \mathfrak{C} \neq 0$. All other harmonics $m \geqslant 1$ might only be included if and only if $\det \mathfrak{C} = 0$. These solvability conditions define sector layouts, where multiple harmonics can be combined (Nec, 2021).

If $k_r/k_\theta \neq 1$, it is of import whether $\tilde{m}$ can take the value $\tilde{m} = 2$ for some m_* in the series in (6). If such m_* exists, i.e. the expression $2\sqrt{k_\theta/k_r}$ gives an integer, m_* becomes the essential harmonic and identical solvability conditions apply. If $\tilde{m} \neq 2 \ \forall m$, the right-hand side vector $\mathbf{r} = \mathbf{0}$ for any m, and any harmonic for which $\det \mathfrak{C} = 0$ is admissible, however such a flow field will only exist for a non-generating medium, i.e. $C^{(n)} = 0 \ \forall n$ and the constants in (6) are redefined to reflect that.

For $m = 0$ the coefficients $b_{i0}^{(n)}$ satisfy

$$b_{i0}^{(n)} = \frac{k_r^{(n)}}{k_r^{(1)}} \, b_{i0}^{(1)}, \quad 1 \leqslant n \leqslant N - 1, \tag{10}$$

leaving $b_{i0}^{(1)}$ as a degree of freedom to be determined from boundary conditions. Due to the rotational invariance of (2a) and periodicity of (6) any sector might be taken to correspond to $n = 1$. Therefore in fact the boundary conditions might be set in any one sector n_*. These might be chosen as

$$p_{n_*}\big|_{r_w} = p_w, \qquad p_{n_*}\big|_{r_x} = p_x, \tag{11}$$

where r_w and r_x are the well and computational domain radii, and p_w and p_x are the constant components of the pressure. Observe that p_w^γ and p_x^γ determine the total mass flux through the circumference of respective circles. In (Nec and Huculak, 2020) it was shown that in most circumstances the θ-dependent component of the pressure is small on $r = r_w$, rendering this somewhat unconventional choice of boundary conditions equivalent to prescribing a constant well head for all practical purposes.

Since $0 < r_w \leqslant r \leqslant r_x < \infty$, formally (6) is bounded. However, as often happens in the course of solution of Sturm-Liouville problems, some eigenfunctions might behave undesirably. Here one must be cautious with the decaying powers of r: the physical dimension of the well is small relative to the domain, whereby with r_x used for non-dimensionalisation $r_w \ll 1$. If one does wish to include harmonics corresponding to large negative powers of r in (6), the magnitude of the constants must be managed accordingly. In most practical cases one would be interested in the flow in the main part of the domain, i.e. $r \sim \mathcal{O}(10)$ and that part of the series would decay quickly. As long as the contiguity ray structure is preserved, solution (6) might be extended to a domain, whose outer perimeter is of an arbitrary shape.

The simplest flow field includes the axially symmetric part and harmonic $m = m_*$ in (6) with $a_{2m_*}^{(n)} = b_{2m_*}^{(n)} = 0$:

$$p_n^\gamma = \frac{C}{4k_r^{(n)}}\left\{b_{1_0}^{(n)} + b_{2_0}^{(n)} \ln r + r^2\Big(a_{1m_*}^{(n)} \sin(m_*\theta) + b_{1m_*}^{(n)} \cos(m_*\theta) - 1\Big)\right\}. \tag{12a}$$

Its candidate stagnation points are given by

$$\theta_{\mathrm{sp}} = \frac{1}{m_*} \arctan \frac{a_{1m_*}^{(n)}}{b_{1m_*}^{(n)}} + \frac{\pi\ell}{m_*}, \quad \ell \in \mathbb{Z}, \tag{12b}$$

$$r_{\mathrm{sp}}^2 = -\frac{b_{2_0}^{(n)}}{2\Big(a_{1m_*}^{(n)} \sin(m_*\theta_{\mathrm{sp}}) + b_{1m_*}^{(n)} \cos(m_*\theta_{\mathrm{sp}}) - 1\Big)}. \tag{12c}$$

Out of the sequence (12b) all points falling within sector n are retained. Then if the right-hand side of (12c) is positive, the pair $\big(r_{\mathrm{sp}}, \theta_{\mathrm{sp}}\big)$ is a valid stagnation point. The locations of these points bear on the set of initial points (r_o, θ_o) for the numerical integration of the velocity field $\mathbf{u}$ to obtain particle pathlines $\big(r(t), \theta(t)\big)$ with t parameterising each curve:

$$\frac{\mathrm{d}r}{\mathrm{d}t} = u = -\frac{k_r^{(n)}}{\mu}\frac{\partial p_n}{\partial r}, \qquad r(0) = r_o, \tag{13a}$$

$$\frac{\mathrm{d}\theta}{\mathrm{d}t} = \frac{v}{r} = -\frac{k_\theta^{(n)}}{\mu}\frac{1}{r^2}\frac{\partial p_n}{\partial \theta}, \qquad \theta(0) = \theta_o. \tag{13b}$$

The union of pathlines connecting the stagnation points delimits the well's basin of attraction and thus forms the zone of influence. Observe that the location of stagnation points is independent of γ, i.e. γ affects the pathline trajectory, but not its issue or terminus point. Thus all examples below were computed with $\gamma = 2$ to avoid uninstructive input variation and allow for a straightforward juxtaposition of flow maps. Upon adjustment of generation rate and well suction to reasonable values for liquids the observed geometry of the zone of influence was not visually distinct from the compressible case $\gamma = 2$. Field (12a) with $k_r/k_\theta = 1$ suffices to recreate a wide variety of zone geometries. The anisotropic case $k_r/k_\theta \neq 1$ constitutes but a slight quantitative variation on the main mechanism of the azimuthal heterogeneity – introducing the factor $\tilde{k}_r^{(n)}\big/\tilde{k}_\theta^{(n)}$ in (8e) – and thus is not instructive. Therefore in all examples below $k_n \overset{\mathrm{def}}{=} k_r^{(n)} = k_\theta^{(n)}$. The fields that included higher harmonics were more difficult to integrate accurately, but did not offer additional qualitative insight.

3 Zone of influence

In the axially symmetric framework the sole component of the velocity vector $\mathbf{u}$ is the radial velocity u, whose only root defines a stagnation point. In the interpretation of the polar geometry this point comprises a closed curve and might thus be construed as a zone of influence. Furthermore, $\mathbf{u}$ is normal to this boundary. Thus the loci of zero velocity and zero normal flux coincide. This degeneracy is the source of all conceptual obstacles associated with the purely radial flow model. When the axial symmetry is broken, this coincidence is resolved: the set of stagnation points contains only isolated points; and the boundary of the zone of influence is a locus of zero normal flux, but its tangential component does not vanish thereon. The curves tracing the boundaries of the attraction / repulsion basins of stagnation points are called separatrices. Their union delineates the zone of influence. The complexity of its shape is determined by the number of subdomains and harmonics in (6) with all but $m = 0$ and $m = m_*$ being optional. When additional harmonics are present, locating stagnation points analytically is impossible, whilst their number increases quickly with m. On the other hand, without the exact location of these points obtaining a well resolved and accurate field of streamlines is extremely difficult, since the integration of (13) in their vicinity is stiff. Pressure field isocontours are easier to visualise and in related geometries indicate that stagnation points due to higher harmonics are located beyond the principal points due to $m = 0$ and $m_* = 2$, and affect the position of the latter only slightly (Awasthi et al., 2023; Tretiakova and Nec, 2023). In this light, for the purpose of tracing the zone of influence it is sufficient to limit the discussion to principal harmonics.

Hereinafter a set of examples of the integration of (13) is given for a variety of geometric layouts. The input parameters are characteristic to medium size landfills (Zeng et al., 2017) and well within the range of typical values for generic porous media studied (Panda and Lake, 1994).

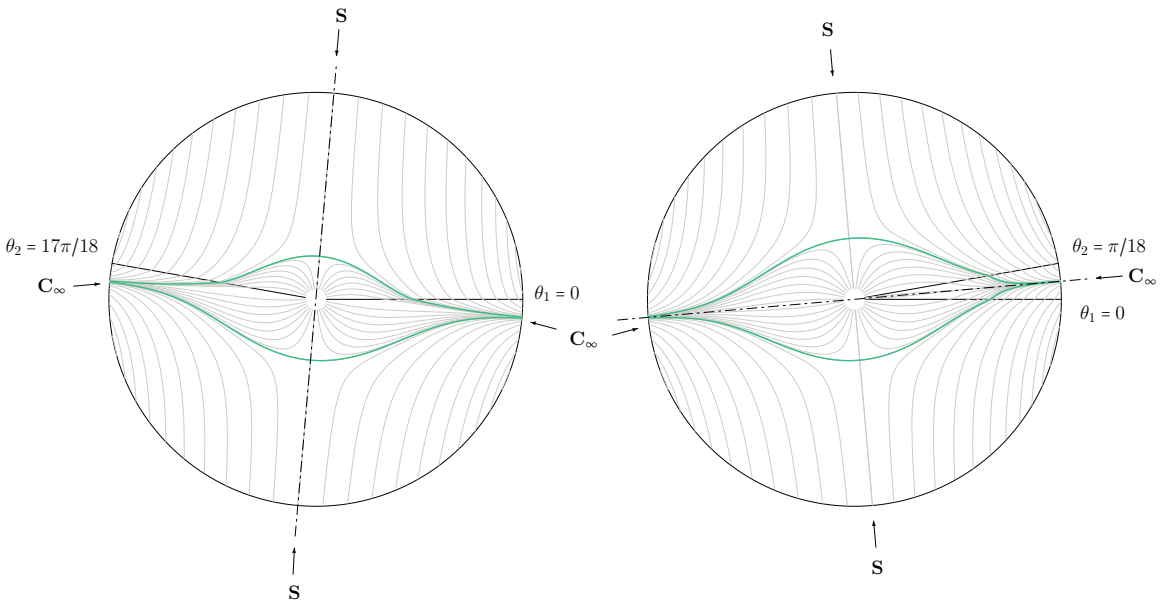

Figure 3: Streamlines (thin grey) and zone of influence (thick green / grey) for $N = 2$ with $\theta_2 - \theta_1 \gtrless \pi/2$. Permeabilities: $k_1 = 2k_2$, $k_2 = 10^{-11}$. Other parameters: $\gamma = 2$, $m_* = 2$, $C = 10^{-11}$, $p_w = -0.1$, $p_x = 1$, $r_w/r_x = 7.62{\times}10^{-4}$, $r_x = 100$m. Follow streamlines marked by arrows to stagnation points: saddle ($\mathbf{S}$), node ($\mathbf{N}$) or cusp at infinity ($\mathbf{C}_\infty$). Streamlines were cut short near the origin for a cleaner exposition.

3.1 Two sectors

The simplest particular case of (12a) is a two sector layout. Equation (2a) is rotationally invariant, whereby one might set $\theta_1 = 0$ without loss of generality. The zone of influence is always eye-shaped. Figure 3 depicts the two possible types of flow maps. When $\theta_2 - \theta_1 > \pi/2$, each sector contains one stagnation point, located on the symmetry line bisecting both sectors (left panel). When $\theta_2 - \theta_1 < \pi/2$, the two stagnation points are located in the larger sector on the line perpendicular to the bisector (right panel). The transition between the two types occurs at $\theta_2 - \theta_1 = \pi/2$ regardless of all other problem parameters (Nec, 2021).

The two stagnation points are of the saddle type. Formally the cusp points (marked by $\mathbf{C}_\infty$) are located at infinity. All four points have $v = 0$, and by (12b) are always $\pi/2$ apart. However, the cusps are not stagnation points: albeit the azimuthal velocity vanishes, the radial velocity is finite and computable in terms of the constants in (12a):

$$\lim_{r\longrightarrow\infty} u = -\lim_{r\longrightarrow\infty} \frac{k_r^{(n)}}{\mu}\frac{\partial p}{\partial r} =$$

$$-\frac{1}{2\mu}\sqrt{Ck_r^{(n)}\left(\frac{a_{1m_*}^{(n)}}{\sin(m_*\theta_{\text{csp}})}-1\right)} = -\frac{1}{2\mu}\sqrt{Ck_r^{(n)}\left(\frac{b_{1m_*}^{(n)}}{\cos(m_*\theta_{\text{csp}})}-1\right)}, \tag{14}$$

where n marks the sector containing the cusp point and θ_{csp} is a root in the set (12b), but not a stagnation point. One of the fractions in (14) might have a zero denominator, but in that case the numerator also vanishes and the ratio remains finite if calculated as a limit expression. Alternatively, the counterpart under the second root would then be well defined, since the sine and cosine functions do not share roots. The expressions under the square roots are positive, giving $u < 0$ and thereby showing that fluid will be collected from that region. Nonetheless, the streamline topology in the vicinity of a cusp closely resembles half a node, making a visual distinction impossible. The presence of such cusp points at infinity is not limited to the two sector layout, cf. figure 7 below. Their occurrence might be regarded as a symmetry artefact similar to the degeneracy observed in purely radial flow. With $N > 2$ the layout symmetry is a necessary, but not sufficient condition for their appearance.

The following important properties were endowed by the heterogeneous model and are generic to all layouts to be discussed hereunder. One, a wide range of reasonable permeability and induced head values yields realistic distances from the well to the nearest boundary of the zone of influence: the order of magnitude spans tens to low hundreds of metres, aligning well with the well design practices in the field. The curves forming the cusps, if present, are virtually closed at only a few multiples of that distance. In that regard defining a cut-off threshold for the cusp would not be conceptually different from doing the same for residual pressure or velocity. Two, low generation rate values do not effect overly optimistic predictions for the zone of collection. Observe that the coefficients corresponding to harmonic $m = 0$ in (6) and (12a) are identical to the integration constants in (3), but the drainage (extraction wells) or dispersal (injection wells) area predicted by the axially symmetric radius of influence (4) might be many orders of magnitude greater. The reason this happens is that the constant preceding the logarithmic term contains two summands: the first depends on the head induced at the well, but not generation rate C, whilst the second is proportionate to C:

$$a = b_0^{(n_*)} = \left(p_x^\gamma - p_w^\gamma + \frac{C}{4k_r^{(n_*)}}\left(r_x^2 - r_w^2\right)\right)\Big/ \ln\frac{r_x}{r_w} \tag{15}$$

with n_* denoting the sector, wherein the boundary conditions were applied. Therefore as $C \longrightarrow 0$, a tends to a constant independent of C, according an arbitrarily large $r_\circledcirc$ in (4). Taking the data in figure (3) as an example (the dimensional quantities therein conform to a gas well of modest capacity), a is estimated as $a \sim \mathcal{O}\left(10^8\right)$, implying $r_\circledcirc \sim \mathcal{O}\left(10^4\right)$, i.e. two orders of magnitude higher than r_x, where the boundary condition p_x was imposed. By contrast, in the heterogeneous model the azimuthal position of stagnation points is fully independent of C and the radial distance depends only weakly thereon via the additive term in (15) with no possibility of infinite growth. This is evident from the formulae given for the particular case (12) and is immediate for the full solution (6) as well. Since the zone of influence is the union of separatrices

connecting the stagnation points, the limit $C \longrightarrow 0$ is proper and results in a finite zone of influence dictated solely by the head induced at the well and mosaic of subdomain permeabilities. Three, the perimeter of the zone of influence is a simple, piecewise smooth contour that encloses a finite area, even in the presence of cusps at infinity. The total mass flux at the well is given by integrating the radial flux component along a positively oriented circular contour c_w:

$$\dot{m} = \oint_{c_w} \rho u r_w \,\mathrm{d}\theta = -\frac{r_w}{\widetilde{\gamma}} \oint_{c_w} k_r \partial_r p^\gamma \,\mathrm{d}\theta = C\left\{\pi r_w^2 - \frac{1}{4}\sum_{n=1}^{N} b_2{}_0^{(n)} \left|\theta_{n+1} - \theta_n\right|\right\}, \tag{16}$$

to wit, $\dot{m}$ is finite as long as r_x in (15) is fixed. Since the mass collected at the well must come solely from within the zone of influence, this proves the finiteness of its area. In fact it might be calculated by $A_z = |\dot{m}|/C$. In (16) $\dot{m} \gtrless 0$ in accordance with the sign of the radial velocity $u \gtrless 0$ with the second summand being dominant by far ($b_2{}_0^{(n)} \gtrless 0$ for extraction and injection wells respectively). The physical meaning of the first summand is exclusion of the well area from the flow field.

The fourth feature regards field observations. One of the common methods to delineate the zone of influence in situ is to measure fluid pressure (residual head relative to the well), velocity or concentration (in the case of aquifer sparging wells) at increasing distances from the well. When the desired quantity falls within a small predefined limit, the corresponding distance is deemed the radius of influence. The flow maps in figure 3, as well as subsequent examples, reveal the mechanism whereby this concept of a threshold often fails: on the boundary marked by the thick green / grey curves the tangential velocity is far from small along most of the curve. The only place where it attenuates is in the vicinity of the two stagnation points. Thus values recorded by a probe situated close to the boundary would not in any way reveal the divide between the well's basin of attraction and repulsion, unless it coincidentally happens to be near one of the stagnation points. If the zone of influence is strongly oblate or the distances from well centre to stagnation points are highly non-uniform (an example of the latter is given later in the right panel of figure 7), the assumption of a circular zone of influence represented by a radius often means data are considered inconsistent and discarded.

The fifth and last feature of note is the break of streamlines' slope at the contiguity rays. This is a consequence of an abrupt change in permeability and has been experimentally documented (Sahu and Flynn, 2015).

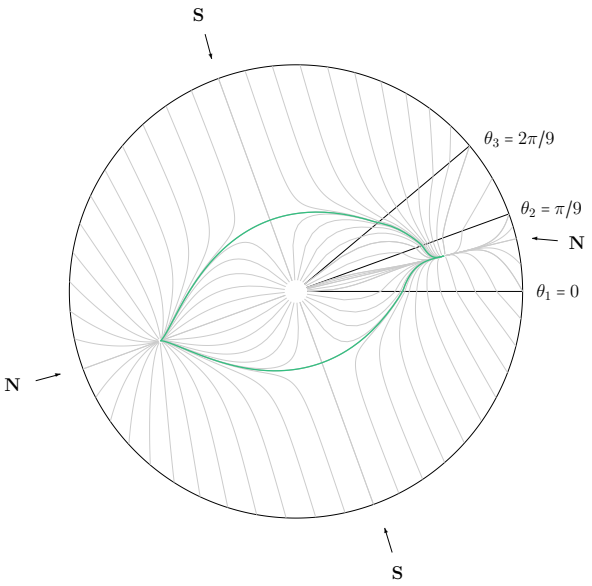

Figure 4: Streamlines (thin grey) and zone of influence (thick green / grey) for $N = 3$ with $\theta_n = (n-1)\pi/9$, $1 \leqslant n \leqslant 3$. Permeabilities: $k_1 = 2k_2$, $k_2 = 10^{-11}$, $k_3 = 3k_2$. All other parameters as in figure 3.

3.2 Three or more sectors

When the combination of geometric layout and corresponding permeabilities harbours no undue symmetry, $N > 2$ configurations offer a fully finite and realistic in size zone of influence. Figure 4 depicts a flow map for an input set differing only slightly from the one in the right panel of figure 3, but the cusps at infinity are replaced by nodes at finite distances. A geometric feature prominent in figure 4 and subsequent examples is the presence of sharp corners in the zone perimeter. This is not an unphysical trait. Observe that the perimeter traced in the figures is for expositional purposes only – it does not constitute a single pathline, but a collection thereof, with no fluid particle's trajectory ever containing a sharp corner except across contiguity rays, where the permeability changes (Sahu and Flynn, 2015). When the zone outline is removed, the behaviour of the pathlines in the vicinity of the apparent sharp corner is smooth.

The shape of the zone of influence might vary quite dramatically. Figures 5–9 give examples of zones that can be broadly categorised as a circle missing a segment, triangle, pear and square. The shape is determined by the constellation of stagnation points, which is sensitive to contiguity angles θ_n and concomitant permeabilities. For instance, the configurations in figures 4 and 5 differ by just one relatively small sector, whose permeability is of a magnitude similar to other sectors. Notwithstanding, the result is a disparate arrangement of stagnation points and a starkly different zone of influence. Figure 7 illustrates sensitivity to permeability alone for two identical layouts: four stagnation points and two cusps (left panel) are replaced by a saddle and cusp (right panel) upon a minor change in k_n values. This further supports the comprehensive measurement uncertainty encountered in large environmental systems such as aquifers and fluid extraction wells, where labile substrate saturation in a part of the domain or its boundary might alter the effective permeability in that azimuthal direction.

A different source of uncertainty is shown in figures 8–9. Observe that some of the nodes in these flow fields are endpoints of long protuberances formed by two separatrices. The length of these needle-like regions roughly equals the distance from well centre to most points on the perimeter of the core zone of influence. In such a case the reading of a probe placed in the vicinity of the needle tip would be congruent with one situated by a less needle-like stagnation point nearer the core zone of influence. When labouring under the assumption of a circular zone of influence, one would be compelled to dismiss at least one of the measurements, since the apparent error would be near 50%. Such protuberances have been associated with an increased medium conductivity in the presence of fractures, cf. figure 3 of (Bradbury and Muldoon, 1994).

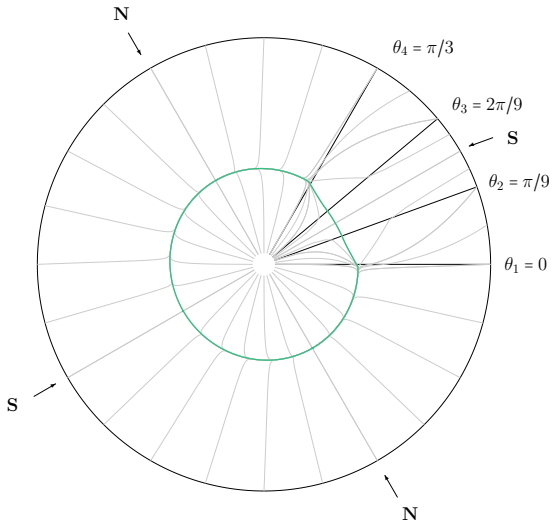

Figure 5: Streamlines (thin grey) and zone of influence (thick green / grey) for $N = 4$ with $\theta_n = (n-1)\pi/9$, $1 \leqslant n \leqslant 4$. Permeabilities: $k_1 = 2k_2$, $k_2 = k_4 = 10^{-11}$, $k_3 = 3k_2$. All other parameters as in figure 3.

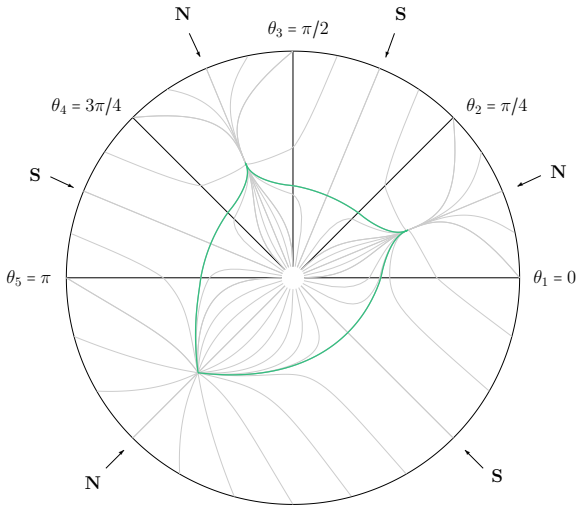

Figure 6: Streamlines (thin grey) and zone of influence (thick green / grey) for $N = 5$ with $\theta_n = (n-1)\pi/4$, $1 \leqslant n \leqslant 5$. Permeabilities: $k_1 = 2k_2$, $k_2 = k_4 = 10^{-11}$, $k_3 = k_5 = 3k_2$. All other parameters as in figure 3.

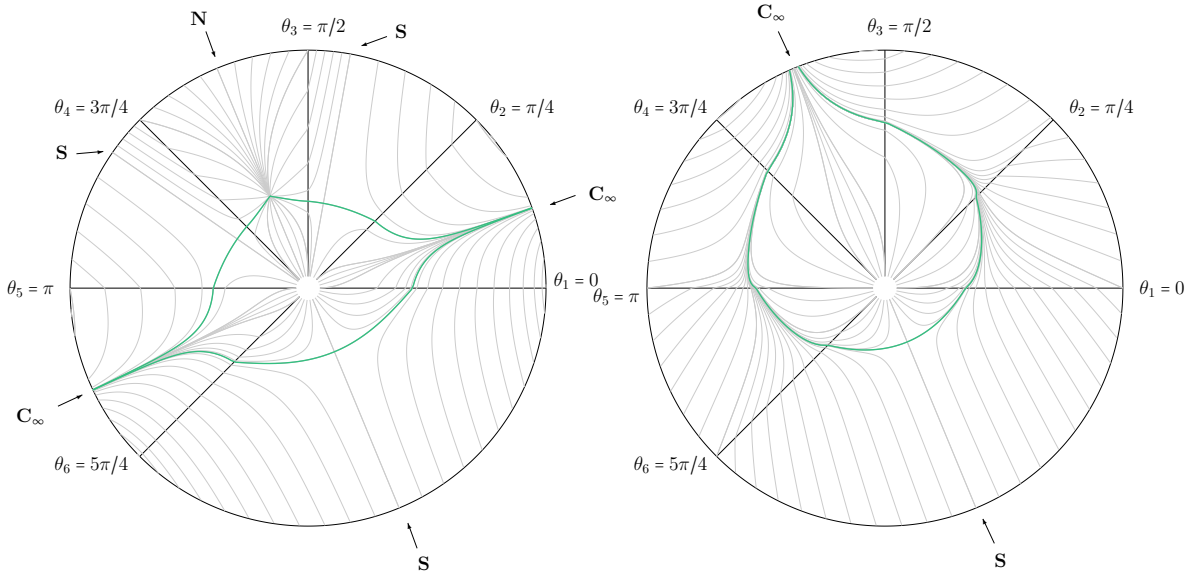

Figure 7: Streamlines (thin grey) and zone of influence (thick green / grey) for $N = 6$ with $\theta_n = (n-1)\pi/4$, $1 \leqslant n \leqslant 6$. Permeabilities: $k_1 = 2k_4$, $k_2 = k_6 = 5 \times 10^{-12}$, $k_3 = k_5 = 3k_4$, $k_4 = 10^{-11}$ (left); $k_1 = 5 \times 10^{-12}$, $k_2 = k_4 = k_6 = 10^{-11}$, $k_3 = k_5 = 3k_2$ (right). Other parameters as in figure 3.

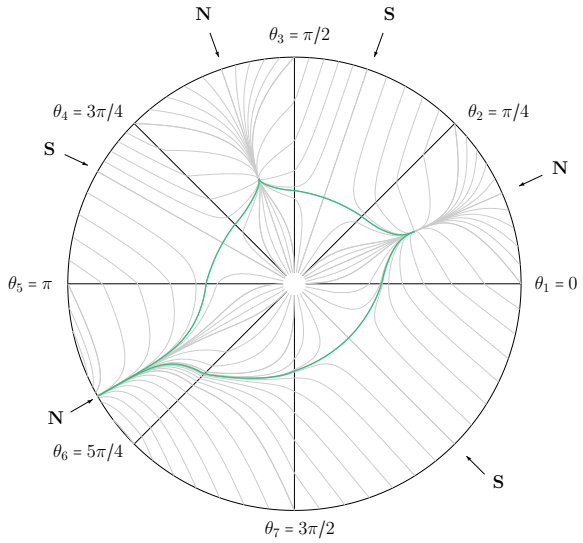

Figure 8: Streamlines (thin grey) and zone of influence (thick green / grey) for $N = 7$ with $\theta_n = (n-1)\pi/4$, $1 \leqslant n \leqslant 7$. Permeabilities: $k_1 = 2k_2$, $k_2 = k_4 = k_6 = 10^{-11}$, $k_3 = k_5 = k_7 = 3k_2$. All other parameters as in figure 3.

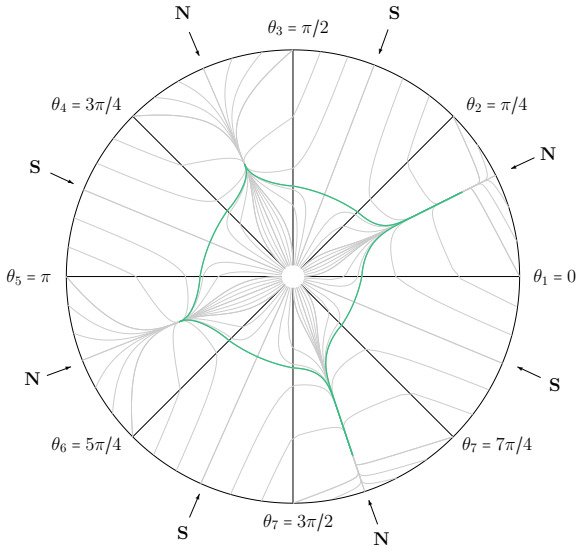

Figure 9: Streamlines (thin grey) and zone of influence (thick green / grey) for $N = 8$ with $\theta_n = (n-1)\pi/4$, $1 \leqslant n \leqslant 8$. Permeabilities: $k_1 = 2k_2$, $k_2 = k_8 = 5 \times 10^{-12}$, $k_3 = k_5 = k_7 = 3k_4$, $k_4 = k_6 = 10^{-11}$. All other parameters as in figure 3.

The area of the zone of influence, on the other hand, is not affected as much by either the layout geometry or the permeability mosaic. This is an important aspect, since the area must be directly related to the injection / extraction energy and in a realistically sound model should not be strongly sensitive to small changes in medium resistance.

4 Conclusion

Historically introducing a representative permeability value when working with a heterogeneous medium has been taken for granted. For wells pumping fluid out of a substrate or injecting fluid thereinto this is inherently connected to the assumption of axial symmetry and grounded in the purpose of the well to effect radial transport. This assumption results in a simple tractable flow model, but is also responsible for a bafflingly inadequate description of the well's reach – an infinite or extremely large radius of influence. In practice not only must the zone of influence be finite, it should not be circular: although ideally a well would induce solely radial transport, in reality the azimuthal motion of the fluid cannot be prevented. This additional dimension of the flow field perceptibly diminishes the fraction of kinetic energy associated with the radial velocity component (Awasthi et al., 2023). Taking this into account remedies the infiniteness of the zone of influence ensuing by a purely radial model and at the same time renders its shape anything but circular. The azimuthal heterogeneity with no structural symmetry is the necessary and sufficient condition to construct a flow solution with a realistic zone of influence.

The separatrix curves connecting the stagnation points form a closed contour that, by the virtue of these lines being streamlines, forms a locus of zero normal flux and the border of the zone of influence. Its shape is sensitive to the particular mosaic of subdomains of distinct permeabilities. In practice preferential directions of flow can open and close swiftly due to fluctuations of water table or more slowly with the settlement of the porous matrix, altering the zone of influence. The introduction of azimuthal heterogeneity provides a unified framework that explains the difficulties encountered in the field when sampling the zone of influence in situ in a variety of applications. Depending on the specific arrangement of permeabilities, one or more of the following factors might be responsible: a markedly oblate zone of influence, needle-like protuberances formed by two separatrices meeting at a node stagnation point, or strong tangential velocities. All three are related, but might not be equally dominant.

One of the model's notable strengths is the weak dependence of stagnation point locations and thence zone of influence on the generation rate C. This ensures that the limit $C \longrightarrow 0$ is proper and thereat the zone of influence is determined, as expected, solely by the head induced at the well and porous medium resistance. Predictions for values typical for wells extracting landfill gas or sparging media surrounding contaminated aquifers range from a few tens of metres to low hundreds, depending on the azimuthal direction. These estimates are realistic and agree with the lateral spacing commonly used in sites containing well networks. To construct an accurate model of a given site one would have to assess effective permeabilities in several azimuthal orientations and partition the domain accordingly.

In practice the permeability within the domain of large environmental applications is an uncertain quantity. Estimating permeability in general is a difficult task, because it represents the overall resistance to flow as evinced by the medium, fluid and system boundaries. Early on it was believed to be derivable exactly for an idealised medium consisting of particles of known shape and size. The original concept due to Kozeny and Carman (Carman, 1937) has seen numerous conceptual extensions, from using a probability distribution to describe the possible variation in particle geometry (Panda and Lake, 1994) through fractals and empirically fit constants (Henderson et al., 2010) and to defining different types of permeability (Sanchez-Villa et al., 2006) that might even depend on the type of flow (Dagan and Lessoff, 2007). In real environmental applications the medium heterogeneity is compounded by the temporal evolution of the flux through the system boundaries due to extraneous factors, affecting the apparent permeability. In particular, a locally sealed boundary perceptibly diminishes the permeability in that azimuthal direction, creating a markedly oblate zone of influence (Bradbury and Muldoon, 1994). The school of thought unifying injection and extraction wells of compressible or incompressible fluid defines an effective apparent permeability as in (1c). In this approach well designers estimate a range of permeabilities encountered at a site and use a steady model to test for the extremes thereof. The advantages of this approach are the necessity of fewer field measurements and a proven conservative design. If measurements with comprehensive azimuthal coverage are available together with some information on the existence and location of preferential directions of flow, the permeabilities might be calibrated to fit these data. However, solving such a reverse engineering problem exceeds the ambit of this study.

A more advanced approach is to model the motion as a stochastic process in a random medium, where the spatial distribution of permeability is a prescribed probability density function, for instance log-Gaussian (Indelman et al., 2006). Extensive measurements are required to substantiate the choice of the distribution and its parameters (Cardiff et al., 2013), and solving the stochastic evolution equation is computationally expensive (Cardiff et al., 2013; Rupert and Miller, 2007). The deviation of the resulting isocontours from the classical circles is directly related to the standard deviation used and is mainly observed away from the well, whereas in its vicinity the shape is close to circular (Brunetti et al., 2022). This methodology is well suited for heterogeneous media without distinctive preferential directions of flow. This situation is more prevalent in applications with incompressible fluids. Permeability to compressible fluids is much more sensitive to the presence of fractures or temporary appearance of partially sealed boundaries that effectively channel the flow in a well defined direction. Such variation cannot be faithfully captured by a probability density function, since the location of these features is deterministic (Gómez-Hernández and Wen, 1998). Its importance is well recognised, encouraging the development of advanced imaging and data fitting techniques (Tahmasebi et al., 2016; Zha et al., 2023). A steady flow with azimuthal variation offers an inexpensive tool to model such systems. Furthermore, under certain conditions it is possible to draw an equivalence between the log-Gaussian stochastic process and a steady flow of an appropriately chosen fixed permeability (Brunetti et al., 2022).

Generalisation of the theory presented herein to other sets of planar curvilinear orthogonal coordinates as well as tridimensional flows in spherical and ellipsoidal geometries is a topic of future study. For instance, eye-shaped domains arise naturally in parabolic coordinates. Since the zone of influence is not a hard boundary of a shape easily described mathematically, setting boundary conditions thereon analytically is impossible. Isocontours inherent to the coordinate system that resemble closely the true shape of the zone of influence would be useful in the development of flow control strategies for the well. Partially penetrating vertical wells with intake at the bottom end (in contrast to continuous intake throughout the well's length) induce a flow field that is better described as spherical instead of cylindrical. Horizontal wells with intake at perforated sections set far apart relative to the pipe radius might be viewed as a sequence of spherical or ellipsoidal zones of influence (Awasthi et al., 2023). The theory is also applicable to unrelated applications of diffusive transport in a heterogeneous medium of much smaller scales, such as drug delivery and diffusant dispersal in polymers upon injection at a source point internal to the domain with the needle acting akin to a well.

References

Agarwal N, Semmens MJ, Novak PJ, Hozalski RM (2005) Zone of influence of a gas permeable membrane system for delivery of gases to groundwater. Water Resour Res 41:W05017

Al-Hussainy R, Ramey Jr HJ, Crawford PB (1966) The flow of real gases through porous media. J Pet Technol 18(05):624–636

Asadi-Aghbolaghi M, Rakhshandehroo GR, Kompani-Zare M (2011) Analytical solutions for the capture zone of a pumping well near a stream. Hydrogeol J 19:1161–1168

Ataie-Ashtiani B, Shafei B, Rashidian-Dezfouli H, Mohamadzadeh M (2012) Capture zone of a partially penetrating well with skin effects in confined aquifers. Transp Porous Media 91:437–457

Awasthi P, Kumar M, Nec Y (2023) Effects of anisotropy in tridimensional diffusion: flow patterns and transport efficiency. SIAM J Appl Math 83(2):460–483

Bakr MI, Butler AP (2004) Worth of head data in well-capture zone design: deterministic and stochastic analysis. J Hydrol 290:202–216

Benner ML, Mohtar RH, Lee LS (2002) Factors affecting air sparging remediation systems using field data and numerical simulations. J Hazard Mater 95:305–329

Bradbury KR, Muldoon MA (1994) Effects of fracture density and anisotropy on delineation of wellhead-projection areas in fractured-rock aquifers. Hydrogeol J 2:17–23

Bresciani E, Shandilya RN, Kang PK, Lee S (2020) Well radius of influence and radius of investigation: what exactly are they and how to estimate them? J Hydrol 583:124646

Brinkman HC (1947) Fluid flow in a porous medium. Appl Sci Res Sec A1 27:143–149

Brunetti GFA, Fallico C, De Bartolo S, Severino G (2022) Well-type steady flow in strongly heterogeneous porous media: an experimental study. Water Resour Res 58(5):e2021WR030717

Cardiff M, Bakhos T, Kitanidis P, Barrash W (2013) Aquifer heterogeneity characterization with oscillatory pumping: sensitivity analysis and imaging potential. Water Resour Res 49(9):5395–5410

Carman PC (1937) Fluid flow through granular beds. Trans Inst Chem Eng 15:150–167

Dagan G, Lessoff SC (2007) Transmissivity upscaling in numerical aquifer models of steady well flow: unconditional statistics. Water Resour Res 43(5):W05431

Durlofsky L, Brady JF (1987) Analysis of the Brinkman equation as a model for flow in porous media. Phys Fluids 30:3329–3341

Frind EO, Molson JW (2018) Issues and options in the delineation of well capture zones under uncertainty. Ground Water 56(3):366–376

Fulks WB, Guenther RB, Roetman EL (1971) Equations of motion and continuity for fluid flow in a porous medium. Acta Mech 12:121–129

Gingras MK, Pemberton SG, Mendoza CA, Henk F (2022) Assessing the anisotropic permeability of Glossifungites surfaces. Pet Geosci 5:349–357

Gómez-Hernández JJ, Wen XH (1998) To be or not to be multi-Gaussian? a reflection on stochastic hydrogeology. Adv Water Resour 21(1):47–61

Halvorsen D, Nec Y, Huculak G (2019) Horizontal landfill gas wells: geometry, physics of flow and connection with the atmosphere. Phys Chem Earth 113:50–62

Henderson N, Brêttas JC, Sacco WF (2010) A three-parameter Kozeny-Carman generalized equation for fractal porous media. Chem Eng Sci 65:4432–4442

Houben GJ (2015) Review: hydraulics of water wells – flow laws and influence of geometry. Hydrogeol J 23:1633–1657

Hyman JD, Karra S, Makedonska N, Gable CW, Painter SL, Viswanathan HS (2015) dfnWorks: a discrete fracture network framework for modeling subsurface flow and transport. Comp Geosci 84:10–19

Indelman P, Lessoff SC, Dagan G (2006) Analytical solution to transport in three-dimensional heterogeneous well capture zones. J Contam Hydrol 87:1–21

Javandel I, Tsang CF (1986) Capture-zone type curves: a tool for aquifer cleanup. Ground Water 24(5):616–625

Kompani-Zare M, Zhan H, Samani N (2005) Analytical study of capture zone of a horizontal well in a confined aquifer. J Hydrol 307:48–59

Kuchuk FJ (2009) Radius of investigation for reserve estimation from pressure transient well tests. Soc Pet Eng 120515:1–23

Lee JH, Woo HJ, Jeong KS, Park KS (2016) The radius of influence of a combined method of in situ air sparging and soil vapor extraction in the intertidal sediments of Gomso Bay on the west coast of South Korea. SpringerPlus 5:1388

Lundegard PD, LaBrecque D (1995) Air sparging in a sandy aquifer (Florence, Oregon, U.S.A.): actual and apparent radius of influence. J Contam Hydrol 19:1–27

McCray JE, Falta RW (1996) Defining the air sparging radius of influence for groundwater remediation. J Contam Hydrol 24:25–52

McCray JE, Falta RW (2005) Numerical simulation of air sparging for remediation of NAPL contamination. Groundwater 35:99–110

Nec Y (2021) Singularities in weakly compressible flow through a porous medium. Fluid Dyn Res 53:045507

Nec Y, Huculak G (2019) Landfill gas flow: collection by horizontal wells. Transp Porous Media 130:769–797

Nec Y, Huculak G (2020) Exact solutions to radial flow in a porous medium with variable permeability. Phys Fluids 32:077108

Panda MN, Lake LW (1994) Estimation of single-phase permeability from parameters of particle-size distribution. Am Assoc Pet Geol Bull 78(7):1028–1039

Pechstein A, Attinger S, Kreig R, Copty NK (2016) Estimating transmissivity from single-well pumping tests in heterogeneous aquifers. Water Resour Res 52(1):495–510

Podgorney, Jr RK, Ritzi RW (1997) Capture zone geometry in a fractured carbonate aquifer. Ground Water 35(6):1040–1049

Rupert CP, Miller CT (2007) An analysis of polynomial chaos approximations for modeling single-fluid-phase flow in porous medium systems. J Comput Phys 226(2):2175–2205

Sahu CK, Flynn MR (2015) Filling box flows in porous media. J Fluid Mech 782:455–478

Sanchez-Villa X, Guadagnini A, Carrera J (2006) Representative hydraulic conductivities in saturated groundwater flow. Rev Geophys 44(3):RG3002

Sobbi FA, Badakhshan A (1996) Radius of investigation for well tests in dual porosity reservoirs. J Can Pet Technol 35(06):PETSOC–96–06–05

Tahmasebi P, Javadpour F, Sahimi M (2016) Stochastic shale permeabiilty matching: three-dimensional charaterization and modeling. Int J Coal Geol 165:231–242

Tretiakova K, Nec Y (2023) Separable solutions to non-linear anisotropic diffusion equation in elliptic coordinates. Philos Trans R Soc A 381:20220077

Vigneault H, Lefebvre R, Nastev M (2004) Numerical simulation of the radius of influence for landfill gas wells. Vadose Zone J 3:909–916

Whitaker S (1986) Flow in porous media I: a theoretical derivation of Darcy's law. Transp Porous Media 1:3–25

Whitaker S (1996) The Forchheimer equation: a theoretical development. Transp Porous Media 25:27–61

Wise WR, Townsend TG (2011) One-dimensional gas flow models for municipal solid waste landfills: cylindrical and spherical symmetries. J Environ Eng 137(6):514–516

Xu Y, van Tonder GJ (2002) Capture zone simulation for boreholes located in fractured dykes using the linesink concept. Water SA 28(2):165–169

Zeng G, Liu L, Xue Q, Wan Y, Ma J, Zhao Y (2017) Experimental study of the porosity and permeability of municipal solid waste. Environ Prog Sustain Energy 36:1694–1699

Zha Y, Cao B, Li F, Ye Q, Zhu S, Zhou W, Xiong R (2023) Pore structure and permeability variations during gas displacement in unconsolidated sandstone reservoirs through CT reconstruction analysis. Geofluids 2023:3701163

Zhang P, Zhang Y, Zhang W, Tian S (2022) Numerical simulation of gas production from natural gas hydrate deposits with multi-branch wells: influence of reservoir properties. Energy 238(A):121738